CrossMark

Tracking timescales of short-term precursors to large basaltic fissure eruptions through Fe–Mg diffusion in olivine

Margaret E. Hartley [a,b,*], Daniel J. Morgan [c], John Maclennan [b], Marie Edmonds [b], Thor Thordarson [d]

[a] *School of Earth, Atmospheric and Environmental Sciences, University of Manchester, Oxford Road, Manchester, M13 9PL, UK*
[b] *Department of Earth Sciences, University of Cambridge, Downing Street, Cambridge, CB2 3EQ, UK*
[c] *School of Earth and Environment, University of Leeds, Leeds, LS2 9JT, UK*
[d] *Institute of Earth Sciences, University of Iceland, Sturlugata 7, 101 Reykjavík, Iceland*

A R T I C L E I N F O

A B S T R A C T

Petrological constraints on the timescales of pre-eruptive crystal storage and magma degassing provide an important framework for the interpretation of seismic, geodetic and gas monitoring data in volcanically active regions. We have used Fe–Mg diffusion chronometry in 86 olivine macrocrysts from the AD 1783–1784 Laki eruption on Iceland's Eastern Volcanic Zone to characterise timescales of crystal storage and transport in the lead-up to this eruption. The majority of these olivines have core compositions of Fo < 76, and rim compositions in the range Fo_{69}–Fo_{74} that are close to equilibrium with the Laki melt. Diffusion modelling using the greyscale intensity of backscattered electron images as a proxy for olivine composition reveals that the most probable Fe–Mg diffusion timescale for Laki olivines is 7.8 days, which reflects the characteristic olivine residence time in the carrier melt prior to eruption. A small population of Fo > 81 olivines record Fe–Mg diffusion timescales of ∼124 days; these crystals are likely to have formed in mid-crustal magma chambers, been transferred to storage at shallower levels and then entrained into the Laki melt prior to eruption. Typical Fe–Mg diffusion timescales of 6–10 days are shorter than the average time interval between discrete episodes of the Laki eruption, indicating variable or pulsed disaggregation of stored crystals into the carrier liquid prior to the onset of each episode. The diffusion timescales coincide with historical accounts of strong and frequent earthquakes in southeast Iceland, which we interpret as being associated with mush disaggregation related to melt withdrawal and the initiation of dyke propagation from a crustal magma reservoir at ∼6 ± 3 km depth to the surface. We calculate pre-eruptive CO_2 fluxes of 2–6 $Mt\,d^{-1}$, assuming a pre-eruptive CO_2 outgassing budget of 189.6 Mt for the Laki eruption and a constant rate of CO_2 release in the 6–10 days preceding each eruptive episode. Our dataset indicates that petrological constraints on the timescales of magmatic processes occurring in the days leading up to historic eruptions may enhance our ability to forecast the onset of future large eruptions, both in Iceland and further afield.

1. Introduction

Many active volcanoes exhibit significant changes in seismicity, ground deformation and gas release in the hours, days and weeks preceding an eruption. One of the principal challenges in modern volcanology is to interpret these signs of volcanic unrest in terms of subsurface processes such as the pre-eruptive storage, transport and degassing of magma. Over the past decade, diffusion chronometry in zoned magmatic crystals has become an indispensable tool for recovering the timescales over which these processes occur (e.g. Costa et al., 2008; Costa and Morgan, 2010). The re-equilibration of different elements across compositional zones can be used to map the passage of crystals through complex magmatic systems, thereby gaining insight into different aspects of magma genesis. Similarly, because different elements diffuse through crystals at different rates, diffusion chronometry is able to recover timescales ranging from minutes to tens or hundreds of years.

Perturbations in the composition, volatile content, temperature, pressure and oxidation state of the magmatic environment are often reflected in the compositional zonation of magmatic crystals, as the equilibrium crystal chemistry responds to these chang-

* Corresponding author at: School of Earth, Atmospheric and Environmental Sciences, University of Manchester, Oxford Road, Manchester, M13 9PL, UK.
E-mail address: margaret.hartley@manchester.ac.uk (M.E. Hartley).

ing magmatic variables. If the responses in crystal chemistry to these magmatic variables are known, either through thermodynamic or experimental models, then the compositional changes across discrete crystal zones can be linked with the magmatic processes responsible for the zonation. By modelling the relaxation of these compositional changes with diffusion chronometry, it is possible to constrain the timescales over which the processes that created the zonation are occurring. This method has been successfully used to determine characteristic crystal residence timescales and magma recharge rates in various volcanic settings, using Sr, Mg and Li diffusion in plagioclase (Zellmer et al., 1999; Costa et al., 2003; Martin et al., 2010; Charlier et al., 2012; Druitt et al., 2012; Saunders et al., 2010); Ba diffusion in sanidine (Morgan et al., 2006); Ni diffusion in olivine (Ruprecht and Plank, 2013); and Fe–Mg diffusion in olivine (Gerlach and Grove, 1982; Costa and Chakraborty, 2004; Martin et al., 2008; Ruprecht and Plank, 2013), clinopyroxene (Morgan et al., 2004; Costa et al., 2013) and orthopyroxene (Allan et al., 2013).

Petrological records of magmatic processes can also be temporally linked with contemporaneous monitoring records in the lead-up to eruptions. Links between petrological observations and seismic, geodetic and/or gas monitoring records have been inferred for eruptions at Mt St Helens (Saunders et al., 2012); Etna (Kahl et al., 2011, 2013) and Ruapehu (Kilgour et al., 2014). Evidence of strong links between diffusion chronometry in magmatic crystals and contemporaneous monitoring records indicates that petrologically determined timescales of magma ascent, mixing and degassing may provide an important framework for the interpretation of seismic, geodetic and gas monitoring data in regions where the last known volcanic eruption occurred before the advent of modern monitoring techniques. One such region is the Laki–Grímsvötn system on Iceland's Eastern Volcanic Zone (EVZ). The most magmatically productive of Iceland's neovolcanic zones, the EVZ accounts for 82% ($\sim$71 km^3) of the magma volume erupted in Iceland since its settlement in AD 874 (Thordarson and Larsen, 2007). Magmatism on the EVZ over the Holocene period has been typified by flood lava eruptions ($>$1 km^3), which include the 8.6 ka Thjorsárhraun, AD 934–938 Eldgjá and AD 1783–1784 Laki eruptions (e.g. Thordarson et al., 2003b; Thordarson and Höskuldsson, 2008). These large-volume, long-lived eruptions have historically produced significant global climatic, environmental and societal impacts (e.g. Thordarson et al., 1996; Larsen, 2000; Thordarson et al., 2001; Thordarson and Self, 2003; Chenet et al., 2005; Oman et al., 2006; Fei and Zhou, 2006; Schmidt et al., 2010), and similar effects may be expected in the event of future flood lava eruptions (Schmidt et al., 2011).

In this study, we use diffusion chronometry to characterise the timescales of crystal storage and transport in the lead-up to the AD 1783 Laki eruption. By comparing petrologically constrained timescales with historical accounts of seismic unrest in the days and weeks preceding eruption onset, we assess the utility of petrological data in interpreting seismic and gas flux monitoring signals in Iceland's Eastern Volcanic Zone.

2. The AD 1783–1784 Laki eruption

The AD 1783–1784 Laki eruption is one of the best-documented small-scale analogues of a flood basalt eruption (e.g. Thordarson and Self, 1993; Thordarson et al., 2003a). Historical accounts report that the eruption was preceded by weak seismicity between 15 and 29 May 1783, and by stronger and more frequent earthquakes between 29 May and 8 June 1783. The eruption began on 8 June 1783 with an explosive event on a short fissure; four days later, lava flows from the Laki vents had reached the lowlands, $\sim$35 km away. Lava continued to flow, with variable magma discharge rates from the vents, until the end of the eruption on 7 February 1784

(Thordarson et al., 2003a). Over the eight months of the eruption, a total of 14.7 km^3 of basaltic lava and $\sim$0.4 km^3 dense rock equivalent of tephra was erupted from the 27 km-long Laki fissure.

The Laki fissure is marked by scoria and spatter cones that define 10 *en echelon* fissure segments which opened sequentially from SW to NE over the course of the eruption. The opening of each fissure segment is considered to be a distinct eruptive episode (Thordarson and Self, 2003). Episodes I–V correspond to the five fissure segments located to the southwest of Laki Mountain, from which the eruption gets its name; episodes VI–X correspond to fissure segments northeast of Laki Mountain. Historical accounts of the eruption report that many of the episodes were preceded by seismic swarms, with earthquake strength and frequency increasing immediately before the opening of each new fissure (Thordarson et al., 2003a). Each episode is thought to have commenced with a short period of explosive activity of sub-Plinian intensity, followed by Hawaiian fire fountaining and lava effusion. The eruptive episodes have been interpreted in terms of variable magma supply rates to the Laki vents (Thordarson and Self, 1993). The chronology of the eruption, reconstructed from the examination of historical accounts and field studies of the preserved volcanic stratigraphy, is summarised in Fig. 1.

2.1. Magmatic mush entrainment at Laki

Whole-rock compositions of Laki lava and tephra samples vary linearly with the total mass fraction of macrocrysts, where the term 'macrocryst' refers to crystals larger than the groundmass and within the size interval $\sim$0.2–10 mm. Samples with the lowest incompatible element concentrations have the highest mass fraction of macrocrysts. This correlation has been explained by the disaggregation and entrainment of a crystal mush into the Laki carrier liquid prior to eruption (Passmore et al., 2012). The importance of disaggregation and entrainment of crystal mushes into magmatic liquids has been explored in a number of recent studies (e.g. Gurenko and Sobolev, 2006; Costa and Morgan, 2010; Thomson and Maclennan, 2013; Moore et al., 2014), several of which have focused on Iceland's Eastern Volcanic Zone (Hansen and Grönvold, 2000; Holness et al., 2007; Halldorsson et al., 2008; Neave et al., 2014).

Geochemical analysis of the Laki crystal cargo, coupled with high-resolution analyses of compositional variability in individual macrocrysts, has provided a detailed record of the processes operating within the Laki magmatic system (Neave et al., 2013). Clinopyroxene-liquid thermobarometry indicates that the bulk of olivine, plagioclase and clinopyroxene crystallisation took place at mid-crustal pressures of 2–5.4 kbar, which is in good agreement with calculated saturation pressures of high-CO$_2$ ($>$1500 ppm CO$_2$) melt inclusions (Hartley et al., 2014). Macrocrysts, and mono- and polymineralic glomerocrysts, are typically surrounded by evolved crystal rims with compositions close to equilibrium with the Laki carrier liquid. These textures imply the formation of polymineralic mushes in the mid-crust, which were then disaggregated and transported to shallower levels where rim crystallisation occurred. The signature of mush addition identified by Passmore et al. (2012) is likely to have been generated at the final depth of equilibration between the melt and the observable rims of olivine, clinopyroxene and plagioclase crystals (Neave et al., 2013). Melt barometry calculations indicate that this occurred at 2 $\pm$ 1 kbar (Neave et al., 2013), but it is not clear whether these pressures represent equilibrium crystallisation as magma temporarily stalled in the shallow crust, or dynamic growth of crystal rims during magma ascent from deeper levels.

The proportion of mush crystals entrained into the Laki carrier liquid is thought to vary over the course of the eruption. Erupted products from episodes VI–X contain larger average mass fractions
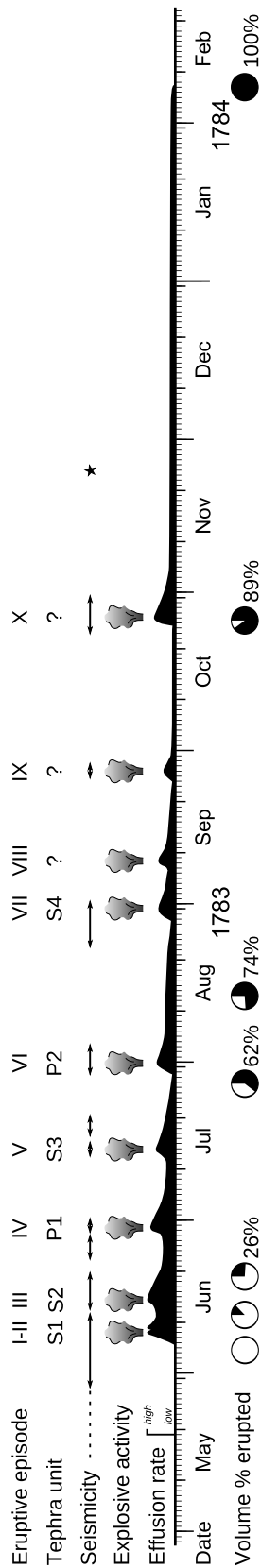
Fig. 1. Schematic illustration of the sequence of events during the Laki eruption, modified after Thordarson et al. (1996). Eruptive episodes I–X and their associated tephra units are shown in the top two rows. 'S' indicates magmatic (strombolian) fall units; 'P' indicates phreatomagmatic fall units. Dashed lines in row 3 indicate weak seismicity; solid arrows indicate periods of strong and frequent seismicity. The star indicates a strong earthquake on 24 November 1783. Explosive activity at the Laki fissures is denoted by the eruption cloud symbols. The effusion rate is shown qualitatively and is not to scale. The volume percentage erupted, shown by the pie charts, was estimated after Thordarson and Self (1993).

of macrocrysts than erupted products from earlier episodes, and also contain higher proportions of more primitive olivine, clinopyroxene and plagioclase crystals: for example, the average olivine composition is Fo_{76} in episodes I–V, and Fo_{80} in episodes VI–VIII (Passmore et al., 2012). This has been interpreted as a larger contribution from the entrained mush assemblage in the latter stages of the eruption.

3. Sample selection

The samples used in this study were collected from the S1, S2 and S3 magmatic tephra units of the Laki eruption, which correspond to episodes I–II, III and V respectively (Fig. 1). Tephra unit nomenclature is adopted from Thordarson and Self (1993), who refer to these units as strombolian tephra. Fresh, glassy material was obtained from proximal fall deposits near the southwestern end of the Laki cone row by digging down through the surface cover. The samples consist of vesicular black scoria lapilli and brown pumice, and contain achneliths and Pele's hair. Olivine macrocrysts comprise $\ll 1\%$ of the S1, S2, and S3 tephra units.

Magmatic tephra samples were selected for this study because olivine macrocrysts in tephra are rapidly cooled upon eruption, which minimises the likelihood of post-eruptive diffusion of Fe and Mg through the olivines. We can therefore assume that Fe–Mg diffusion profiles in olivines from tephra samples preserve information about the timescales of sub-surface crystal storage or transport. By contrast, olivines from lava samples are likely to have experienced post-eruptive Fe–Mg diffusion during insulated transport within the Laki lava, meaning that diffused profiles in these olivines cannot be reliably associated with sub-surface magmatic processes. A comparison of zoning in olivines from tephra and lava samples in order to examine the effects of post-eruptive thermal history on recovered diffusion timescales will be the subject of a future study.

Phreatomagmatic tephra units in Laki's proximal tephra sequence contain up to 15 wt.% lithic fragments (Thordarson and Self, 1993). These lithics are mainly basalt and hyaloclastite, and many are crystal-rich. To avoid the accidental inclusion of xenocrystic olivines in our study, we focused only on magmatic tephra units.

4. Methodology

4.1. Analytical methods

Pale green, unaltered olivine macrocrysts in the size range 250 μm to 1 mm were hand-picked from crushed magmatic tephra samples, mounted in resin and polished to expose a flat crystal surface. High-resolution backscattered electron (BSE) images of these olivines were obtained using an FEI Quanta 650 FEG-ESEM scanning electron microscope at the University of Leeds. The BSE images were used to identify crystals preserving compositional zonation. Greyscale intensity profiles perpendicular to crystal edges were extracted from BSE images using ImageJ software. Greyscale profiles were then calibrated by analysing the major element compositions of the olivines (e.g. Martin et al., 2008), using a Cameca SX100 electron microprobe (EPMA) at the University of Cambridge. EPMA analyses were performed using a 15 keV accelerating voltage, 20 nA beam current and 1 μm spot size, with measurements made at $\sim$5 μm intervals.

Crystallographic axis orientations were determined by electron backscatter diffraction (EBSD) at the University of Leeds. The EBSD patterns were processed using Oxford Instruments software and used to calculate the angles between crystallographic axes and the measured BSE greyscale and EPMA compositional traverses (e.g. Costa and Chakraborty, 2004). This allowed us to correct for the

strongly anisotropic diffusion of Fe and Mg in olivine, where diffusion along the [001] crystallographic orientation is around six times faster than along [100] or [010] (Nakamura and Schmalzried, 1983; Dohmen and Chakraborty, 2007).

4.2. Modelling Fe–Mg interdiffusion in olivine

Best-fit diffusion profiles to the calibrated BSE/EPMA traverses were modelled using a method parallel to that described by Allan et al. (2013), adapted for Fe–Mg interdiffusion in olivine. Because Fe–Mg diffusion in olivine is anisotropic and composition-dependent (Dohmen and Chakraborty, 2007), the more compositional contrast that a grain displays, the more a diffused profile will differ from the typical symmetrical diffusion sigmoid and the more markedly asymmetric the resulting diffusion. Due to these feedbacks, a database of simulated diffusion profiles obeying composition-dependent diffusion under a one-dimensional geometry was calculated using finite-difference software (D.J. Morgan, unpublished). Composition-dependent diffusion in 1-D has the property that all profiles generated for a given set of boundary conditions (temperature, oxygen fugacity, anisotropy, composition) are self-similar in time. For example, diffusion after 4 time units will be twice as wide as for 1 time unit, but in all other respects the diffusion sigmoids are geometrically identical. A simple stretch factor applied to the length of the profile can therefore be used to bring profiles into congruency. If the boundary conditions for the observed diffused profile are known, then the curve that has the correct shape and hence the correct diffusional behaviour can be selected from the database of previously calculated 1-D models. To achieve this, the distance between the 20th and 80th percentiles in the distribution of compositions along the observed profile are extracted and scaled to the appropriate model curve from the database using the correct stretch factor, before the observed and model profiles are overlain, setting the 50th percentile of both profiles to $x = 0$. The stretch factor scaling law is then used to relate time in the model profile to the diffusion time elapsed in the sample. This method provides a rapid and repeatable procedure where modelling difficulties can be quickly identified and evaluated. Further details of the modelling approach are provided in a supplementary file.

For each diffused profile in the Laki olivines, an appropriate boundary condition (stranded profile or buffered edge) was selected based upon the shape of the profile and its location within or at the edge of the crystal. Greyscale and EPMA traverses with profile shapes not consistent with the diffusive modification of an initially step-wise boundary, such as linear compositional gradients perpendicular to the crystal edge, were discarded. For some crystals we modelled profiles along two different crystallographic directions to confirm the expected diffusion anisotropy and verify the absence of growth effects in the observed profile. The majority of profiles had good to near-perfect fits to the model data. Profiles with poor fits between model and data were excluded from further analysis.

Calculations were performed using a magmatic temperature of $1150 \pm 30\,°C$ and an oxygen fugacity of 1 ± 0.5 log units below the QFM buffer. The selected temperature is consistent with temperatures of 1150–1160 °C obtained by clinopyroxene-liquid thermometry on clinopyroxene rims thought to have crystallised during the final stages of melt storage and crystal-melt equilibration prior to eruption (Neave et al., 2013). The assumed oxygen fugacity corresponds to $Fe^{3+}/\Sigma Fe \approx 0.12 \pm 0.02$ and is consistent with previous estimates of oxygen fugacity in Icelandic magmatic systems (e.g. Maclennan, 2008; Neave et al., 2013). Published $Fe^{3+}/\Sigma Fe$ values for Icelandic basalts range from 0.08 (Breddam, 2002) to 0.15 (Óskarsson et al., 1994).

The largest sources of uncertainty in constraining appropriate values for D_{Fe-Mg}, and in the associated error in the modelled diffusion timescales, are the values adopted for temperature and oxygen fugacity. Uncertainties were estimated using a *Monte Carlo* simulation to propagate a temperature uncertainty of $\pm 30°$ and fO_2 uncertainty of ± 0.5 log units onto the calculated diffusivities. We also take into account uncertainties on the profile shapes (i.e. the compositional reliability of the BSE images) and the profile length (based upon the reliability of the magnification provided by the SEM imaging, which is taken as $\pm 2\%$). The average uncertainty on each calculated timescale is 0.67 $\log_{10}$ units (2σ).

We also investigated the effect of variable magmatic temperatures on calculated diffusion timescales. To do this, we calculated reverse fractional crystallisation paths for the Laki carrier melt, taking the average composition of Laki tephra glass (Hartley et al., 2014) as a starting melt composition. Calculations were performed using Petrolog3 (Danyushevsky and Plechov, 2011), which makes use of published mineral-melt equilibria to calculate the melt and crystal compositions and liquidus temperatures under specified conditions. Calculations were performed at 1.5 kbar and fO_2 of $\Delta QFM-1$, using the Danyushevsky (2001) mineral-melt models for plagioclase and clinopyroxene, and the Gaetani and Watson (2002) model for olivine. Measured core compositions of Laki olivines were matched with olivine compositions calculated by the reverse fractional crystallisation model, and the crystallisation temperature for that olivine composition was then taken as the magmatic temperature to be used in the diffusion calculation for that crystal. Temperatures obtained from the reverse crystallisation model ranged from 1113 to 1175 °C (average $1145 \pm 10°$), with a near-linear correlation between temperature and olivine forsterite content.

5. Results

5.1. Compositions of Laki olivines

We obtained a total of 103 high-resolution BSE images and EPMA traverses from 86 olivine macrocrysts: 52 olivines and 60 profiles from the S1 magmatic tephra, 4 olivines and 4 profiles from S2, and 30 olivines and 39 profiles from S3. This includes three traverses measured perpendicular to the edges of melt inclusions hosted within olivine macrocrysts. Olivine core compositions range from Fo_{70} to Fo_{86}, while rim compositions range from Fo_{68} to $Fo_{81.5}$ (Fig. 2). These compositions are comparable with data from previous studies (Métrich et al., 1991; Thordarson et al., 1996; Guilbaud et al., 2007; Passmore et al., 2012; Neave et al., 2013; Hartley et al., 2014). The majority of the olivines (73%) have core compositions of $Fo < 76$. All but five of the 28 olivine macrocrysts with core compositions of $Fo > 76$ are from the S1 tephra unit. The majority of rim compositions fall within the range Fo_{69}–Fo_{74}, and are in or close to equilibrium with the Laki carrier melt (Guilbaud et al., 2007; Neave et al., 2013; Hartley et al., 2014). These crystal rims may have formed during the final stages of magma storage and crystallisation prior to eruption, or may have formed during magma ascent.

The majority of Laki olivines display simple normal zoning comprising a more forsteritic core and a less forsteritic rim (Fig. 3). Five profiles display reverse zonation; four of these are in olivines from the S3 tephra (Fig. 2). Eleven olivines preserve evidence of three compositional zones. Three of these macrocrysts have highly forsteritic cores ($Fo > 83$) with zones becoming progressively less forsteritic towards the crystal rim. The remaining eight macrocrysts have $Fo \sim 75$ cores surrounded by thin (5–15 μm) zones of a less forsteritic composition (Fo_{72} to Fo_{69}), with the outermost zone being no more than 8 μm wide and on average slightly more forsteritic (Fo_{71}–Fo_{73}).
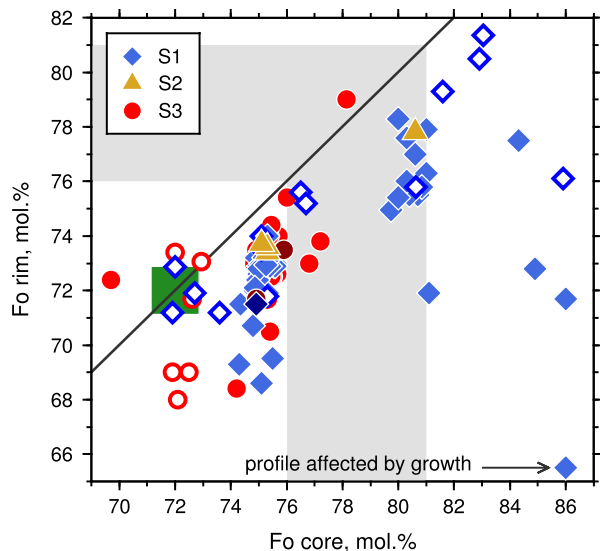
Fig. 2. Core and rim compositions of olivine macrocrysts from the S1, S2 and S3 Laki magmatic tephra units. Most olivines show simple normal zoning, and plot below the grey 1:1 line. Five olivines show reverse zonation, and plot above the 1:1 line. Filled symbols represent olivines with only two compositional zones (core and rim); open symbols indicate the minimum and maximum forsterite contents for diffused profiles within olivines that display three compositional zones. Dark filled symbols indicate diffusion profiles adjacent to melt inclusions. The green square shows the composition of olivine in equilibrium with the Laki carrier melt. The majority of olivines have rim compositions of Fo₇₄–Fo₇₁ that are close to equilibrium with this carrier melt. Olivines with core compositions of Fo ≥ 79 are found almost exclusively in the S1 tephra. The grey shading shows the subdivision of olivine compositions into Fo < 76, 76 ≤ Fo < 81 and Fo ≥ 81 as used in the text. (For interpretation of the references to color in this figure legend, the reader is referred to the web version of this article.)

5.2. Diffusion modelling results

Our calibrated BSE/EPMA profiles reveal that the majority of Laki olivines preserve evidence of partial re-equilibration via diffusive exchange of Fe and Mg between crystal cores and rims. Diffused profile lengths ranged from 3 to 460 μm, with an average length of 74 μm. Fe–Mg diffusion timescales, calculated assuming a temperature of $1150 \pm 30\,°C$ and fO_2 of $\Delta QFM\text{-}1 \pm 0.5$, are summarised in Fig. 4 and Table 1. We find no systematic relationship between olivine size and length of diffused profile or diffusion timescale. For some olivines, particularly those with high compositional contrast between core and rim (e.g. core Fo_{81}, rim Fo_{76}), Ca and Ni diffusion were also resolvable. We calculated Ca and Ni diffusion timescales for a small number of olivines; the recovered timescales were similar to those obtained for Fe–Mg diffusion. See supplementary material for further details.

For over 80% of the olivines analysed we calculated Fe–Mg diffusion timescales of less than 30 days (Fig. 4a). The probability distribution curve for all Laki olivines, taking into account the thermal and fO_2 uncertainties, shows a peak at a timescale of 7.8 days (Fig. 4d). A 1σ uncertainty of 0.33 $\log_{10}$ units indicates that this peak corresponds to a timescale range of 3.6–16.8 days. Peaks in the probability distributions of olivines from the S1 and S3 tephras are identical within error to the peak in the overall probability distribution (Fig. 4d, Table 1), indicating that olivines from the S1 and S3 tephras experienced similar magmatic environments prior to eruption. The scarcity of olivine macrocrysts in the S2 tephra unit precludes the calculation of a statistically significant peak in the S2 probability distribution; however, our data suggest that S2 olivines are likely to preserve a similar distribution of diffusional timescales to olivines from S1 and S3.

The Laki tephra samples are dominated by olivines with core compositions of Fo < 76 that are close to equilibrium with the

Laki carrier liquid. It is therefore unsurprising that the peak in the probability distribution for Fo < 76 olivines of 6.5 days is identical within error to the probability distribution for all Laki olivines (Fig. 4e, Table 1). Probability distributions for more forsteritic olivine populations show that Fe–Mg diffusion in more primitive macrocrysts occurred over longer timescales. The most primitive olivine population, with core compositions of Fo ≥ 81, has a peak in its probability distribution at a timescale of 124 days (Fig. 4e). Diffusion timescales in $76 \leq Fo < 81$ olivines are more variable than for the Fo ≥ 81 olivine population; nonetheless there is a peak in the probability distribution at 22 days.

It is likely that the more primitive olivine macrocrysts were stored for part of their history in a hotter magmatic environment than the Fo < 76 population. Their longer diffusional timescales could then be an artefact caused by an underestimation of the magmatic temperature. We therefore re-calculated all diffusional timescales using crystallisation temperatures from our reverse fractional crystallisation model (Section 4.2). The results are summarised in Fig. 4 and Table 1. For olivines with compositions of Fo > 76, the diffusion timescales modelled using crystallisation temperatures calculated with the Gaetani and Watson (2002) olivine-melt equilibrium model are shorter than when a fixed temperature of 1150° is used. This is most noticeable for the most primitive olivines. The calculated timescales for $76 \leq Fo < 81$ olivines are less variable, resulting in a better-defined peak in the probability distribution. However, the timescales calculated using fixed and variable magmatic temperatures are identical within error for all tephra units and olivine populations (Table 1). This demonstrates that the longer diffusion timescales in more primitive olivine macrocrysts are a real feature of our dataset.

Diffused profiles adjacent to the three melt inclusions record Fe–Mg diffusion timescales of 11.7, 21.7 and 46.6 days. The inclusions are hosted in olivines with core compositions of Fo_{75} (two olivines) and Fo_{76}; the olivine compositions directly adjacent to the inclusions were $Fo_{71.5}$ (two inclusions) and $Fo_{73.5}$.

6. Discussion

6.1. Mush disaggregation and crystal entrainment

The most primitive olivines are the most long-lived crystals in the Laki magmatic system, recording Fe–Mg diffusion timescales of ∼130 days between their Fo > 81 cores and more evolved rims with compositions of Fo_{75}–Fo_{77}. Long diffusion timescales are not recorded in the population of olivines with Fo ∼ 76 core compositions. This observation can be explained if liquids percolating through mushy horizons in the lower crust entrained olivines with Fo > 81 cores and transported them to shallower melt and/or mush horizons in the mid-crust (Fig. 5). In the case of Laki, this carrier liquid crystallised new olivines with compositions close to Fo_{76}, while rims of Fo ∼ 76 olivine formed around pre-existing Fo > 81 olivine cores. The crystals then settled into a new mush horizon, where local diffusion acted both to homogenise the core compositions of individual olivines, and to reduce the compositional variance of the mush pile, creating a compositional peak corresponding to the mean forsterite content of the olivines within the mush pile (Thomson and Maclennan, 2013). This process is likely to have produced the population of relatively uniform olivines with Fo_{75}–Fo_{76} cores that we observe. Previous studies noted peaks in the distribution of Laki olivine core compositions at Fo ∼ 85 and Fo ∼ 78 (e.g. Guilbaud et al., 2007; Thomson and Maclennan, 2013), which may have been generated during previous periods of crystal storage in mush horizons within the lower and mid-crust. Diffusive Fe–Mg exchange between Fo > 81 cores and Fo ∼ 76 rims can be used to constrain
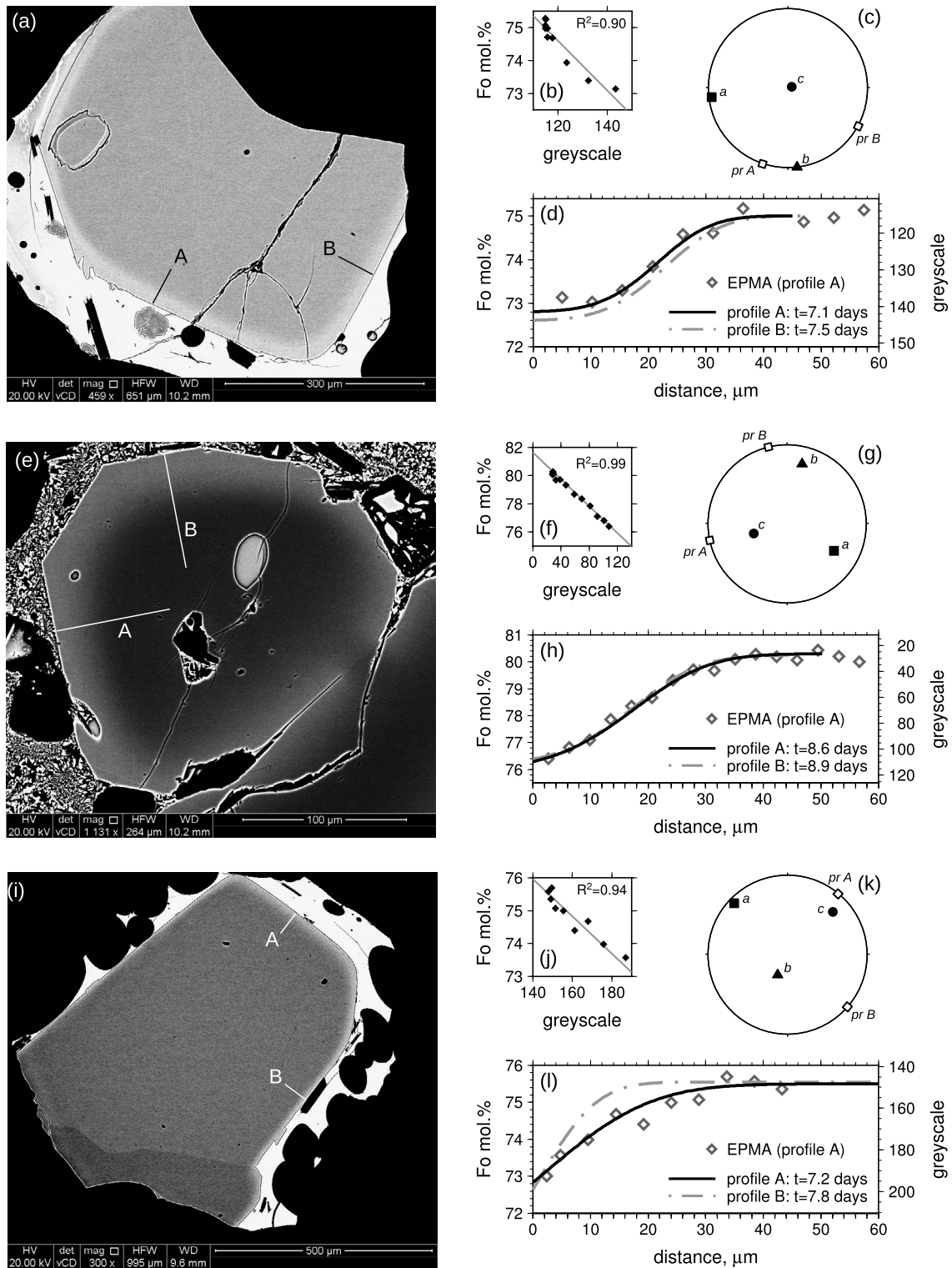
Fig. 3. Representative backscattered electron (BSE) images of olivines; calibrations between forsterite content and BSE greyscale; upper hemisphere projections of the orientation of the electron microprobe profiles (pr) relative to crystallographic axes (*a*, *b* and *c*) of the olivine crystal; and diffusion model fits to compositional profiles. Lines on the BSE images show the position of the traverses. (a–d) and (e–h) Normally zoned olivines from the S1 tephra unit. (i–l) Normally zoned olivine from the S3 tephra. The symbols in (d), (h) and (l) show electron microprobe (EPMA) analyses along the profiles labelled 'A'; solid black lines show best-fit diffusion models to the EPMA and greyscale data for these profiles. Grey dashed lines show diffusion models to profiles labelled 'B' which are fitted using greyscale data alone. Profiles along different crystallographic directions within the same olivine confirm the expected diffusion anisotropy and recover near-identical timescales.

olivine residence times in the mid-crustal mush pile. The characteristic residence timescale is on the order of ∼130 days, although the range of residence timescales (∼15–380 days; Fig. 4) reflects the diversity of crystal histories within the mush pile. Diffused

profiles adjacent to melt inclusions correspond to Fe–Mg exchange between the host crystal and a high-forsterite rim on the inclusion wall formed in response to post-entrapment cooling and crystallisation. This post-entrapment cooling event may reflect the addition
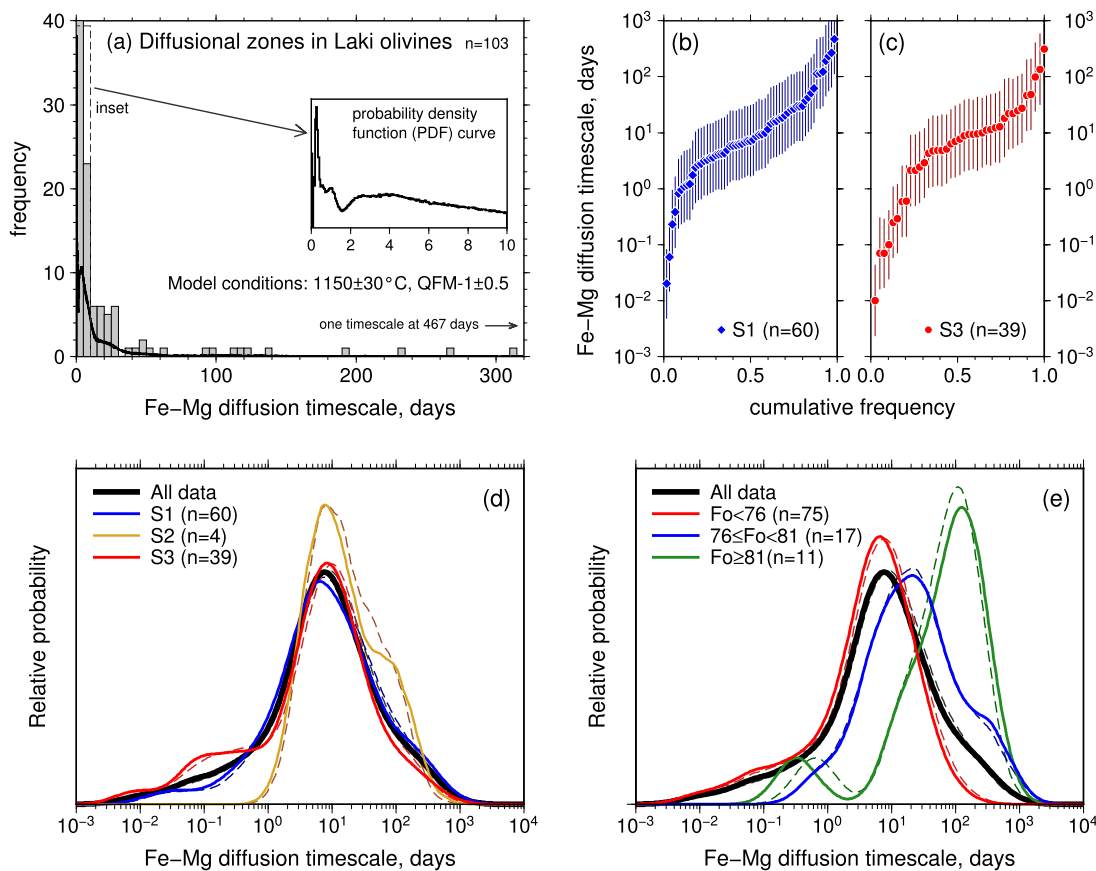
Fig. 4. (a) Histogram showing the range and frequency of Fe–Mg diffusion timescales for Laki olivines. The black line denotes the probability distribution for the entire population ($n = 103$) taking into account the associated errors on each timescale, which were calculated assuming a temperature uncertainty of $\pm 30\,°C$ and oxygen fugacity uncertainty of ± 0.5 log units. (b) and (c) Individual timescales and absolute uncertainties for olivines from the S1 and S3 tephra units, with associated error based on propagation of temperature and oxygen fugacity uncertainties. (d) Kernel density estimates, with bandwidth 0.1, of probability distributions, taking into account the temperature and oxygen fugacity uncertainties. Note the logarithmic scale. Olivines are grouped by tephra unit. The thin dashed lines show diffusion timescales and probability distributions calculated using olivine crystallisation temperatures obtained from a reverse fractional crystallisation model calculated with the olivine–liquid equilibrium model of Gaetani and Watson (2002). (e) Kernel density estimates of probability distributions, with olivines grouped by composition.

Table 1

Most probable Fe–Mg diffusion timescales for Laki olivines, determined from peaks in probability distribution curves (Fig. 4) and taking into account a temperature uncertainty of $\pm 30\,°C$ and oxygen fugacity uncertainty of ± 0.5 log units. The second column shows diffusional timescales calculated assuming a fixed magmatic temperature of $1150 \pm 30\,°C$. The third column takes variable magmatic temperatures into account, with diffusion models run using olivine crystallisation temperatures obtained from a reverse fractional crystallisation model calculated with the olivine–liquid equilibrium model of Gaetani and Watson (2002). Numbers in parentheses show the 1σ range of timescales.

	Fe–Mg diffusion timescale, days	
	$T = 1150\,°C$	$T = $ G&W2002
S1	6.5 (3.0–14.0)	7.4 (3.5–16.0)
S2	7.8 (3.6–16.8)	8.2 (3.8–17.6)
S3	8.5 (4.0–18.4)	9.8 (4.6–21.1)
Fo < 76	6.5 (3.0–14.0)	7.8 (3.6–16.8)
$76 \leq$ Fo < 81	21.5 (10.0–46.3)	21.5 (10.0–16.3)
Fo $\geq$ 81	124 (57.7–268)	108 (50.2–233)
All olivines	7.8 (3.6–16.8)	9.0 (4.2–19.3)

of inclusion-bearing crystals to the mush pile; diffusion timescales suggest that this occurred within a timeframe of 10–100 days prior to eruption.

Olivines stored in the magmatic mush were subsequently introduced into a different magmatic environment, where Fo $\sim$ 76 cores were overgrown by rims with compositions of Fo_{72}–Fo_{73}. These rim compositions are close to equilibrium with the Laki carrier liquid. The characteristic diffusion timescale of 6–10 days between Fo $\sim$ 76 olivine cores and Fo $\sim$ 73 olivine rims therefore indicates that olivine crystals from the mush horizon were entrained into the Laki carrier liquid 6–10 days before eruption onset.

The diffusion timescale of 6–10 days is common to olivine macrocrysts from the S1 and S3 tephra units, which are associated with eruptive episodes I–II and V. These episodes commenced on 8 June and 9 July 1783 respectively, and were separated in time by a period of 31 days (Fig. 1). This means that most of the olivine macrocrysts from the S3 tephra could not yet have been resident in the Laki carrier liquid when the episode I–II eruptions commenced. Furthermore, the characteristic diffusion timescale of 6–10 days is shorter than the 15-day average time interval between consecutive episodes of the Laki eruption (the minimum interval is 1 day between episodes I and II; the maximum is 28 days between episodes IX and X). Our data therefore support a model of variable or pulsed disaggregation of mush crystals into the Laki carrier liquid prior to eruption (Fig. 5).

It is likely that the rate of magma ascent slowed or stalled as each episode progressed, resulting in partial settling of the crystal cargo and temporary clogging of the magmatic plumbing system. Accumulated crystals plus a small volume of carrier liquid would then be stored in the shallow crust for the short time between the end of one eruptive phase and the commencement of the next, during which time continued growth of evolved crystal rims and the formation of new crystals might occur. A new batch of ascending magma could thus entrain a population of crystals with compositions near equilibrium with the Laki carrier liquid, in addition to carrying a cargo of crystals from deeper in the crust.

A repeated pattern of magma stalling, crystal settling and growth, and subsequent re-entrainment, could explain the episodicity of the Laki eruption.

Olivine core compositions of Fo > 76 are almost exclusively confined to the S1 tephra (Fig. 2). While it is possible that the scarcity of Fo > 76 olivines in our S2 and S3 tephra samples stems from a sampling bias and might not persist if more crystals were measured, Passmore et al. (2012) obtained a similar distribution of olivine compositions in lava samples from eruptive episodes I, III and V which suggests that this compositional distribution is a real feature of the first half of the Laki eruption. The apparently abrupt disappearance of Fo > 76 olivines from the Laki magma following episode I is not consistent with the continuous dissolution of high-Fo olivines in the Laki carrier liquid, since this process would suggest a gradual decline in the abundance of Fo > 76 olivines between episodes I and V. It therefore appears that the entrainment of Fo > 76 olivine macrocrysts into the Laki carrier liquid was more efficient during episodes I–II than during episodes III–V. One possible explanation is that the mush horizon was somewhat stratified, with the more primitive olivines located in the lower part of the mush. Vigorous convection and mush overturn at the start of the eruption could facilitate the entrainment of more primitive olivines from lower parts of the mush into the carrier liquid, while less vigorous convection prior to episodes III–V might entrain only Fo $\leq$ 76 olivines from the upper part of the mush pile (Fig. 5). If this is the case, then vigorous convection and entrainment of primitive mush crystals must have resumed after episode V, since olivine macrocrysts in lavas from episodes VI–X have more primitive average olivine core compositions of Fo_{78}–Fo_{80} (Passmore et al., 2012). Alternatively, the crystal mush formed an elongate and laterally heterogeneous body beneath the Laki fissure, with the more primitive olivines being concentrated in the north-eastern part of the mush horizon underlying eruptive fissures VI–X. A third possibility is that the compositional distribution of crystals in the erupted products of each episode reflects a progressively changing compositional distribution in the population of stalled and accumulated crystals in the shallow crust.

Although there is a trade-off between the Laki mush liquid composition and the mush porosity (Passmore et al., 2012), the mush liquid is constrained to be ferrobasaltic in composition with Mg# $\sim$ 0.3, with a corresponding porosity of 45–65%. It is therefore plausible that some Laki olivines acquired thin, low-forsterite rims while in contact with the evolved mush liquid, with these low-forsterite zones being themselves overgrown when the olivines were entrained into the Laki carrier liquid prior to eruption. We documented a small number of olivines preserving more than one compositional zone, where the intermediate zones between core and rim had compositions between Fo_{68} and Fo_{72}. We suggest that these intermediate, low-forsterite compositional zones are indicative of these olivines having interacted with an evolved liquid within the mush pile. Ferrobasaltic liquids with Mg# $\sim$ 0.3 are expected to be in equilibrium with Fo $\sim$ 60 olivine. If the intermediate zones were formed when the crystals were in contact with the mush liquid and had initial compositions of Fo $\sim$ 60, then significant Fe–Mg exchange is required for these zones to reach their measured compositions of Fo_{68}–Fo_{72}. For Laki olivines with low-forsterite Fo_{60} zones with initial thickness 5–12 μm, typical diffusion timescales of 1–10 days are required for the intermediate zones to reach their measured compositions. The thinnest Fo_{60} zones ($\leq$5 μm) may be completely obscured by Fe–Mg diffusion within 8–10 days, i.e. on similar timescales to typical crystal residence within the Laki carrier liquid. This may explain why so few Laki olivines preserve compositional evidence of interaction with an evolved mush liquid.

6.2. Diffusion timescales and the onset of seismicity

The Laki eruption was preceded by 11 days of strong and frequent earthquakes which began on 29 May 1783 and continued until eruption onset on 8 June 1783. Historical accounts also report weak tremors in the Skaftártunga region between 15 and 29 May 1783 (Thordarson and Self, 1993). The records of pre-eruptive seismicity are comparable with our characteristic diffusion timescales of 6–10 days for the entrainment of olivines into the Laki carrier liquid. The diffusion timescales in Laki olivines are also comparable with the thirteen days of earthquake movement on the Bárðarbunga volcanic system that preceded the eruption at Holuhraun, which began on 29 August 2014 (Sigmundsson et al., 2014). We therefore suggest that the onset of strong and frequent seismicity in southeast Iceland prior to the Laki eruption was associated with mush disaggregation related to melt withdrawal, and the initiation of dyke propagation to the surface.

6.3. Implications for pre-eruptive CO_2 outgassing

Fe–Mg diffusion timescales in Fo < 76 olivines provide an estimate of the likely timescales of pre-eruptive CO_2 outgassing. In this section we explore the possible implications of our modelled diffusion timescales on pre-eruptive CO_2 fluxes for various outgassing scenarios.

The total CO_2 mass release associated with the Laki eruption has been calculated as 304 Mt (Hartley et al., 2014) (Fig. 6a). However, CO_2 solubility in basaltic melt is strongly pressure-dependent (e.g. Shishkina et al., 2010). To determine the CO_2 mass available for pre-eruptive outgassing during the final stages of magma ascent, it is therefore necessary to constrain the pressure from which the magma ascended. In the discussion below, we assume that the majority of pre-eruptive CO_2 loss occurs at $\sim$2 $\pm$ 1 kbar, i.e. after the last equilibration of melt with olivine, plagioclase and clinopyroxene (Neave et al., 2013). Just over 60% of the total Laki CO_2 budget, 189.6 Mt, is therefore associated with 'shallow' pre-eruptive and/or syn-eruptive outgassing (Fig. 6a). This approach provides conservative estimates of the pre-eruptive CO_2 outgassing budgets and fluxes, since it does not account for CO_2 loss at pressures >2 kbar.

Two equilibrium endmember scenarios of CO_2 outgassing from the Laki magma can be considered. Firstly, CO_2 may be outgassed as soon as it is exsolved (Fig. 6b). Some 40% of the total CO_2 mass release from the Laki magma would then be lost during deep (i.e. $\gtrsim$2 kbar) passive degassing, with the remaining $\sim$60% outgassed during the final stages of magma ascent (i.e. $\lesssim$2 kbar). Secondly, CO_2 may be outgassed only once magma is erupted from the vents (Fig. 6c). This could be achieved if CO_2 remained saturated or supersaturated in the melt. However, low CO_2 concentrations and CO_2/Nb < 100 in Laki melt inclusions hosted in Fo < 80 olivines provide evidence that the Laki magma was not supersaturated in CO_2 prior to eruption (Hartley et al., 2014); similarly, very low CO_2 concentrations in Laki tephra glass demonstrate that the carrier liquid was not CO_2-supersaturated at the point of eruption. Alternatively, exsolved bubbles of CO_2 may remain in the magma without coalescing and escaping by buoyant rise to the surface. Exsolved bubbles only rise buoyantly once they are large enough to overcome the yield strength of the melt; this is facilitated by bubble coalescence and bubble expansion during magma ascent. For basaltic melts, bubbles are expected to rise buoyantly through a moving liquid once they exceed $\sim$1 cm in diameter (Vergniolle and Jaupart, 1986).

Historical accounts of the Laki eruption have been used in combination with field data to estimate the volumetric output, and hence the eruption rate, during different periods of the Laki eruption (Thordarson and Self, 1993) (Fig. 1). This information can be
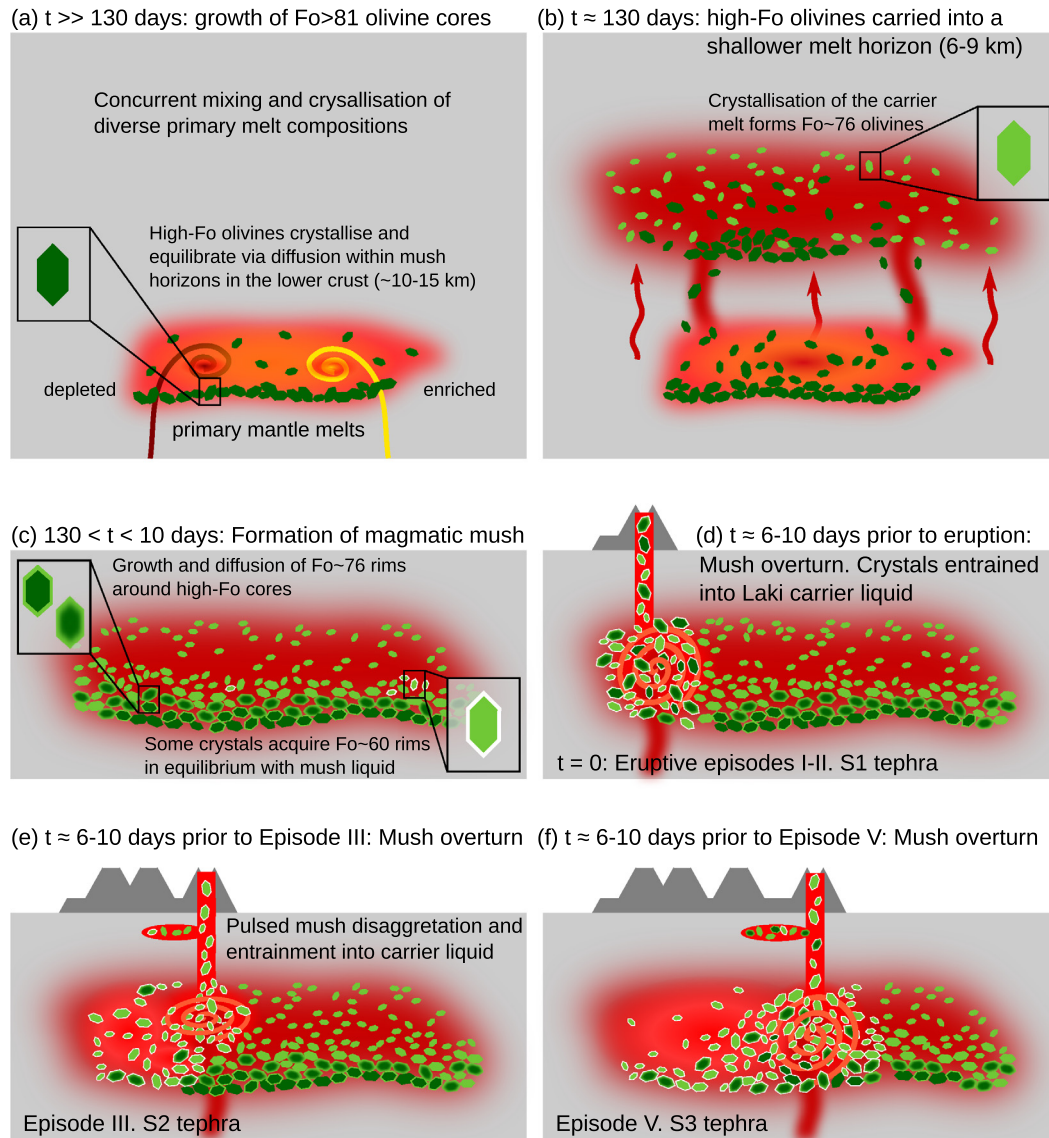
Fig. 5. Schematic cartoon (not to scale) summarising the processes operating in the lead-up to the Laki eruption. Only olivine crystals are shown. (a) Fo > 81 olivines crystallise and equilibrate with one another in mush horizons in the lower crust. (b) Around 130 days before eruption onset, liquids percolating through the mushy lower crust entrain Fo > 81 olivines and transport them to a shallower level in the mid-crust. These liquids crystallise Fo ∼ 76 olivines, while Fo ∼ 76 rims form around the Fo > 81 olivine cores. (c) Crystals settle into a mush horizon in the mid-crust. Olivines equilibrate with one another in the mush pile, producing uniform Fo ∼ 76 olivine cores. Diffusive Fe–Mg equilibration occurs between high-forsterite olivine cores and Fo ∼ 76 rims. Rare olivines may acquire thin Fo ∼ 60 rims when in contact with an evolved mush liquid. (d) Around 6–10 days prior to eruption onset, ascent of the Laki carrier liquid through the mush horizon results convection, overturn and partial disaggregation and entrainment of mush crystals into the Laki melt, including olivines with Fo > 81 core compositions. Seismicity is associated with mush disaggregation related to melt withdrawal, and the onset of dyke propagation to the surface. Eruption commences; eruptive episodes I–II form the S1 tephra. (e) At 6–10 days prior to episode III, a new phase of magma ascent entrains a new population of Fo ∼ 76 olivines into the carrier liquid. Crystals from the previous episode, now stalled in the shallow crust, may also be entrained. Episode III forms the S2 tephra. (f) At 6–10 days prior to episode V a third population of Fo ∼ 76 olivines is entrained into the carrier liquid. Episode V forms the S3 tephra. During episodes VI–X, higher proportions of mush crystals are entrained into the Laki carrier liquid, including crystals with more primitive compositions. This may reflect a changing compositional distribution of stalled crystals in the shallow crust.

used to gain insight into the likely CO_2 mass flux associated with different episodes of the eruption. We have calculated the CO_2 mass release for different periods of the Laki eruption, assuming that the rate of CO_2 release is directly proportional to the magma discharge rate (Table 2; see supplementary file for further details). Episodes IV–V, which together produced ∼36% of the total erupted volume, are associated with the largest CO_2 mass release.

For both our equilibrium outgassing scenarios we calculate the predicted daily CO_2 mass release rate associated with pre-eruptive outgassing, assuming a total CO_2 budget of 189.6 Mt. For the first outgassing scenario we assume a pre-eruptive outgassing period of 6–10 days, which would suggest that CO_2 outgassing occurred in response to overturn, mush disaggregation and melt withdrawal

from the Laki magmatic system. We also assume that the pre-eruptive outgassing rate remains constant over these 6–10 days. Calculations indicate that the pre-eruptive CO_2 mass release was approximately equal for all ten episodes, at ∼2–6 Mt d^{-1} (Table 2). A possible exception is the CO_2 release prior to episodes VII–IX with lower calculated pre-eruptive CO_2 release of 0.9–1.5 Mt d^{-1}; however, given the assumptions made in the calculations, it is difficult to assess whether this difference is significant.

In the alternative outgassing scenario where CO_2 is outgassed only once magma is expelled from the vents, the expected daily CO_2 mass release is directly proportional to the volumetric eruption rate. Eruption rates are expected to be greatest at the start of each episode and thereafter to reach a steady state or to grad-
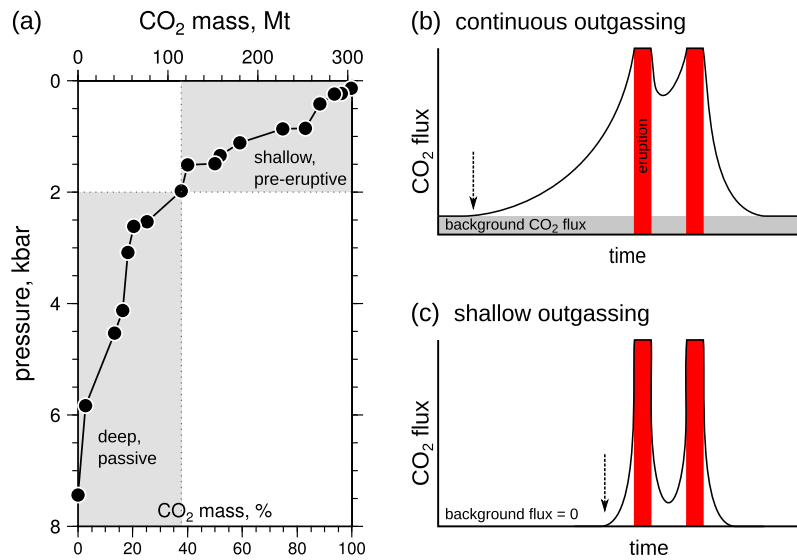
Fig. 6. (a) Cumulative CO_2 release from the Laki magma as a function of pressure, as determined from melt inclusion CO_2 saturation pressures, modified from Hartley et al. (2014). Shaded areas show the potential CO_2 mass release associated with 'deep' ($\gtrsim 2$ kbar) and 'shallow' ($\lesssim 2$ kbar) degassing. 'Shallow' degassing is assumed to occur after the last equilibration of melt with olivine, plagioclase and clinopyroxene at $\sim 2 \pm 1$ kbar (Neave et al., 2013). There is no statistically significant correlation between host olivine composition and melt inclusion CO_2 saturation pressure (Hartley et al., 2014). (b) and (c) Cartoons illustrating potential changes in CO_2 flux in the lead-up to eruption, for different CO_2 outgassing scenarios. (b) CO_2 is outgassed as soon as it is exsolved from the magma, which contributes to a continuous background CO_2 flux. In the lead-up to eruption an increase in CO_2 flux is expected as magma ascends to towards the vents. (c) CO_2 is outgassed only in the shallow crust and primarily at the vents. The background CO_2 flux is close to zero, and no significant pre-eruptive CO_2 flux is expected. Black dashed arrows indicate when the CO_2 flux first rises above the background level.

Table 2

Magma discharge and CO_2 mass release during the Laki eruption. Time periods are based on those given in Table 6 of Thordarson and Self (1993), who calculate the volumes associated with different episodes based on the known location of the lava flow front on the given dates. LEF is the length of eruptive fissure active during each time period. Volumes are given as dense rock equivalent, and include an estimate of the volume of tephra erupted during each time period. VER is the volumetric eruption rate, calculated assuming a constant eruption rate across each time period. VER_F is the volumetric eruption rate scaled to the length of the active fissure. CO_2 mass release is assumed to be proportional to the volumetric output; column 'CO_2 mass' gives the total CO_2 budget associated with each time period. 'CO_2 MRR' is the pre-eruptive CO_2 mass release rate assuming that pre-eruptive degassing occurs in the 6–10 days prior to each episode. 'CO_2 MRR_F' is the pre-eruptive CO_2 mass release rate per metre of active fissure per episode.

Episode(s)	Start	End	Time (days)	LEF (m)	Volume (km^3)	VER (m^3 s^{-1})	VER_F (m^3 m^{-1} s^{-1})	CO_2 mass (Mt)	CO_2 MRR (Mt d^{-1})	CO_2 MRR_F (kg m^{-1} s^{-1})
I–II	8 Jun	12 Jun	5	2200	2.0	4514	2.05	24.5	3.4–5.7[a]	14–23[a]
I–II	13 Jun	14 Jun	2	2800	0.75	4340	1.55	9.4		
III	15 Jun	18 Jun	4	4500	1.2	3472	0.77	15.1	1.5–2.5	4–6
IV–V	19 Jun	27 Jul	39	5200	5.4	1603	0.31	67.8	3.4–5.7	15–25
VI	28 Jul	9 Aug	12	4600	1.9	1833	0.40	23.9	2.4–4.0	6–10
VII–IX	10 Aug	29 Oct	80[b]	7600	2.2	318	0.04	27.6	0.9–1.5	4–7
X	30 Oct	7 Feb	101[b]	2500	1.7	195	0.08	21.3	2.1–3.6	10–16
Total			243		15.1			189.6[c]		

[a] Episodes I and II were separated temporally by one day and so are treated as a single episode in these calculations.

[b] Includes periods of minimal activity at the vents.

[c] Total CO_2 output associated with degassing at pressures >2 kbar (Hartley et al., 2014).

ually decline. It is difficult to quantitatively assess the volumetric eruption rate during each episode, so we calculate an average (i.e. constant) eruption rate for each time period of the eruption (Table 2). The syn-eruptive CO_2 release appears to decrease exponentially over the course of the eruption (Fig. 7). In this endmember outgassing scenario the pre-eruptive CO_2 flux is zero.

Our calculated CO_2 flux of 2–6 Mt d^{-1} prior to the Laki eruption is significantly greater than present-day CO_2 emissions of at least 44 t d^{-1} from Hekla volcano (Ilyinskaya et al., 2015). The CO_2 degassed at the summit of Hekla may represent just 1–6% of the total annual CO_2 release from Hekla (Ilyinskaya et al., 2015), with the remaining CO_2 being transported by the Hekla groundwater system (Flaathen et al., 2009). In the extreme situation that a similar proportion of volcanic CO_2 from Laki were transported via groundwater circulation, then CO_2 outgassing at the surface would be reduced to 20–360 kt d^{-1}. This is far in excess of background CO_2 emissions from diffuse soil degassing in Iceland, which have

been measured at 13.9 t d^{-1} from the Reykjanes geothermal area (Fridriksson et al., 2006), and 1526 $\pm$ 160 t d^{-1} from Hengill volcanic system (Hernández et al., 2012).

Laki CO_2 fluxes of 20–360 kt d^{-1} are comparable to the 11 kt d^{-1} of CO_2 measured at Stromboli prior to an explosive paroxysm on 15 March 2007, and elevated CO_2 fluxes of >6 kt d^{-1} between 8 and 14 March 2007 (Aiuppa et al., 2010). These CO_2 outputs are significantly greater than Stromboli's typical background CO_2 flux of ~ 0.5 kt d^{-1} (Aiuppa et al., 2010). The elevated CO_2 fluxes at Stromboli were interpreted in terms of degassing from magma stored at ~ 4 km depth, and indicate that continuous CO_2 flux monitoring may allow the accurate forecasting of explosive eruptions at basaltic volcanoes. Our calculations suggest that pre-eruptive CO_2 fluxes at Laki were at least one order of magnitude higher than that measured at Stromboli. This highlights the potential utility of gas flux monitoring in forecasting future eruptions at central volcanoes in Iceland, where the location of the
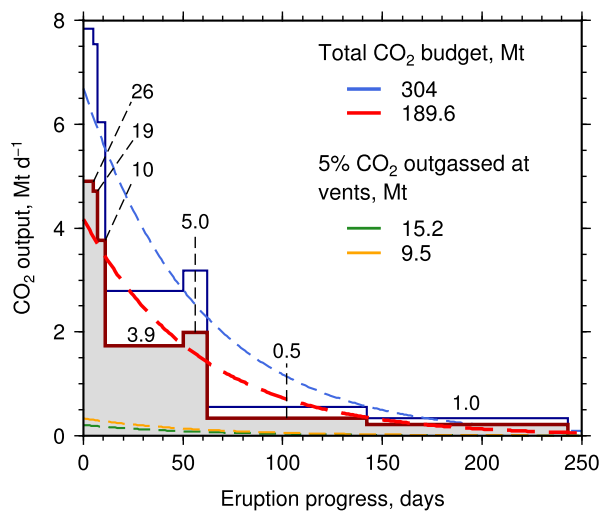
Fig. 7. Histogram of calculated average daily CO_2 output from the Laki vents, assuming that CO_2 outgassed syn-eruptively at the vents. The syn-eruptive CO_2 outgassing rate is assumed to be constant over each time period (time periods used for the calculations are the same as those in Table 2). The histogram shaded in grey assumes that only deep CO_2 is outgassed from the magma, leaving a total CO_2 budget of 189.6 Mt for syn-eruptive outgassing. Numbers above the bars state the average CO_2 mass release per metre of active fissure, in $kg\,m^{-1}\,s^{-1}$. The blue histogram assumes a total CO_2 budget of 304 Mt, i.e. that no CO_2 is outgassed prior to eruption. For each outgassing scenario, the coloured dashed lines show the average daily CO_2 output for each CO_2 budget, and display an exponential decrease in CO_2 flux over the course of the eruption. Green and orange lines show the expected CO_2 output assuming that only 5% of volcanic CO_2 is outgassed at the vents. (For interpretation of the references to color in this figure legend, the reader is referred to the web version of this article.)

volcanic edifice and eruptive vent is confined to a small geographic area. An equivalent scenario at Laki is if pre-eruptive outgassing is focused at the 27 km-long eruptive fissure, such that outgassing rates can be scaled to estimate the CO_2 mass flux rate per unit length of active fissure (Table 2).

If diffuse CO_2 emissions occur across a wide area, elevated CO_2 fluxes in the lead-up to eruption will be more difficult to detect and monitor. For Laki, pre-eruptive CO_2 fluxes of 20–360 $kt\,d^{-1}$ in the 6–10 days prior to eruption occurring within an area extending 5 km in every direction from the Laki fissure yield predicted CO_2 fluxes between 1900–3200 $gm^{-2}\,d^{-1}$ (episodes VII–IX) and 9400–16,000 $gm^{-2}\,d^{-1}$ (episodes I–II). Doubling the area of diffuse degassing reduces the CO_2 flux per unit area by half. Modern gas monitoring instruments are capable of detecting CO_2 fluxes on the order of 10–100 $gm^{-2}\,d^{-1}$ (e.g. Ilyinskaya et al., 2015), which suggests that long-term gas monitoring on Iceland's active neovolcanic zones is possible, provided that the level of background CO_2 flux is well characterised.

7. Conclusions

We have used Fe–Mg diffusion chronometry in 86 olivine macrocrysts from the S1, S2 and S3 tephra units of the AD 1783–84 Laki eruption to determine the timescales of crystal storage and transport in the lead-up to this eruption. Fo < 76 olivines preserve characteristic diffusion timescales of 6–10 days, which reflects the timescale of overturn and entrainment of crystals into the Laki carrier liquid prior to eruption. These timescales are shorter than the average time interval between consecutive episodes of the Laki eruption, and support a model of variable or pulsed mush disaggregation and entrainment of stored crystals over the course of the eruption. Our dataset indicates that magmatic systems feeding large basaltic fissure eruptions experience rapid changes in the days leading up to eruption, which may provide important short-term precursors to eruption onset.

Petrological constraints on the timescale of mush disaggregation are consistent with the timing of seismic activity in the lead-up to the Laki eruption. Fe–Mg diffusion timescales of 6–10 days coincide with the onset of strong and frequent earthquakes in the Skaftártunga region, which we interpret as the onset of mush disaggregation and melt withdrawal, and the initiation of dyke propagation to the surface. Our dataset therefore indicates that diffusion chronometry provides an important constraint on the timing of magma intrusions or recharge events, which can be detected by seismic and/or geodetic monitoring. Similarly, CO_2 outgassing from magma storage chambers beneath Laki most probably yielded a pre-eruptive CO_2 mass release of up to 2–6 $Mt\,d^{-1}$, assuming a constant rate of CO_2 release over the 6–10 days preceding each episode. Measurable CO_2 fluxes may be reduced if a significant proportion of volcanic CO_2 is transported via groundwater circulation, and by diffuse outgassing across a large area surrounding the eventual eruptive vent. For Laki, diffuse pre-eruptive CO_2 emissions could have been as low as 2000–3000 $gm^{-2}\,d^{-1}$; however, CO_2 outputs of this magnitude are readily detectable by modern monitoring techniques. This highlights the potential for CO_2 flux monitoring during periods of seismic unrest to enhance the accuracy of eruption forecasting for future large Icelandic eruptions.

Our results indicate that petrological constraints on the timescales of magmatic processes occurring in the days leading up to historic eruptions may enhance our ability to interpret modern seismic, geodetic and gas monitoring data in terms of pre-eruptive magma storage, transport and degassing in active volcanic systems, both in Iceland and further afield.

Appendix A. Supplementary material

Supplementary material related to this article can be found online at http://dx.doi.org/10.1016/j.epsl.2016.01.018.

References

Aiuppa, A., Burton, M., Caltabiano, T., Giudice, G., Guerrieri, S., Liuzzo, M., Murè, F., Salerno, G., 2010. Unusually large magmatic CO_2 gas emissions prior to a basaltic paroxysm. Geophys. Res. Lett. 37, L17303.

Allan, A.S.R., Morgan, D.J., Wilson, C.J.N., Millet, M.A., 2013. From mush to eruption in centuries: assembly of the super-sized Oruanui magma body. Contrib. Mineral. Petrol. 166, 143–164.

Breddam, K., 2002. Kistufell: primitive melt from the Iceland mantle plume. J. Petrol. 43, 345–373.

Charlier, B.L.A., Morgan, D.J., Wilson, C.J.N., Wooden, J.L., Allan, A.S.R., Baker, J.A., 2012. Lithium concentration gradients in feldspar and quartz record the final minutes of magma ascent in an explosive supereruption. Earth Planet. Sci. Lett. 319, 218–227.

Chenet, A.L., Fluteau, F., Courtillot, V., 2005. Modelling massive sulphate aerosol pollution, following the large 1783 Laki basaltic eruption. Earth Planet. Sci. Lett. 236, 721–731.

Costa, F., Andreastuti, S., Bouvet de Maisonneuve, C., Pallister, J.S., 2013. Petrological insights into the storage conditions, and magmatic processes that yielded the centennial 2010 Merapi explosive eruption. J. Volcanol. Geotherm. Res. 261, 209–235.

Costa, F., Chakraborty, S., 2004. Decadal time gaps between mafic intrusion and silicic eruption obtained from chemical zoning patterns in olivine. Earth Planet. Sci. Lett. 227, 517–530.

Costa, F., Chakraborty, S., Dohmen, R., 2003. Diffusion coupling between trace and major elements and a model for calculation of magma residence times using plagioclase. Geochim. Cosmochim. Acta 67, 2189–2200.

Costa, F., Dohmen, R., Chakraborty, S., 2008. Time scales of magmatic processes from modeling the zoning patterns of crystals. Rev. Mineral. Geochem. 69, 545–594.

Costa, F., Morgan, D., 2010. Time constraints from chemical equilibration in magmatic crystals. In: Dosseto, A., Turner, S.P., van Orman, J.A. (Eds.), Timescales of Magmatic Processes: From Core to Atmosphere. Wiley–Blackwell, pp. 125–159.

Danyushevsky, L.V., 2001. The effect of small amounts of H_2O on crystallisation of mid-ocean ridge and backarc basin magmas. J. Volcanol. Geotherm. Res. 110, 265–280.

Danyushevsky, L.V., Plechov, P., 2011. Petrolog3: integrated software for modeling crystallization processes. Geochem. Geophys. Geosyst. 12, 1–32.

Dohmen, R., Chakraborty, S., 2007. Fe–Mg diffusion in olivine II: point defect chemistry, change of diffusion mechanisms and a model for calculation of diffusion coefficients in natural olivine. Phys. Chem. Miner. 34, 409–430.

Druitt, T.H., Costa, F., Deloule, E., Dungan, M., Scaillet, B., 2012. Decadal to monthly timescales of magma transfer and reservoir growth at a caldera volcano. Nature 482, 77–80.

Fei, J., Zhou, J., 2006. The possible climatic impact in China of Iceland's Eldgja eruption inferred from historical sources. Clim. Change 76, 443–457.

Flaathen, T.K., Gislason, S.R., Oelkers, E.H., Sveinbjörnsdóttir, Á.E., 2009. Chemical evolution of the Mt. Hekla, Iceland, groundwaters: a natural analogue for CO_2 sequestration in basaltic rocks. Appl. Geochem. 24, 463–474.

Fridriksson, T., Kristjánsson, B.R., Armannsson, H., Margrétardóttir, E., Ólafsdóttir, S., Chiodini, G., 2006. CO_2 emissions and heat flow through soil, fumaroles, and steam heated mud pools at the Reykjanes geothermal area, SW Iceland. Appl. Geochem. 21, 1551–1569.

Gaetani, G.A., Watson, E.B., 2002. Modeling the major-element evolution of olivine-hosted melt inclusions. Chem. Geol. 183, 25–41.

Gerlach, D.C., Grove, T.L., 1982. Petrology of Medicine Lake Highland volcanics: characterization of endmembers of magma mixing. Contrib. Mineral. Petrol., 147–159.

Guilbaud, M.N., Blake, S., Thordarson, T., Self, S., 2007. Role of syn-eruptive cooling and degassing on textures of lavas from the AD 1783–1784 Laki eruption, South Iceland. J. Petrol. 48, 1265–1294.

Gurenko, A.A., Sobolev, A.V., 2006. Crust-primitive magma interaction beneath neo-volcanic rift zone of Iceland recorded in gabbro xenoliths from Midfell, SW Iceland. Contrib. Mineral. Petrol. 151, 495–520.

Halldorsson, S.A., Óskarsson, N., Grönvold, K., Sigurdsson, G., Sverrisdóttir, G., Steinthórsson, S., 2008. Isotopic-heterogeneity of the Thjorsa lava: implications for mantle sources and crustal processes within the Eastern Rift Zone, Iceland. Chem. Geol. 255, 305–316.

Hansen, H., Grönvold, K., 2000. Plagioclase ultraphyric basalts in Iceland: the mush of the rift. J. Volcanol. Geotherm. Res. 98, 1–32.

Hartley, M.E., Maclennan, J., Edmonds, M., Thordarson, T., 2014. Reconstructing the deep CO_2 degassing behaviour of large basaltic fissure eruptions. Earth Planet. Sci. Lett. 393, 120–131.

Hernández, P.A., Pérez, N.M., Fridriksson, T., Egbert, J., Ilyinskaya, E., Thárhallsson, A., Ívarsson, G., Gíslason, G., Gunnarsson, I., Jónsson, B., Padrøn, E., zn Melián, G., Mori, T., Notsu, K., 2012. Diffuse volcanic degassing and thermal energy release from Hengill volcanic system, Iceland. Bull. Volcanol. 74, 2435–2448.

Holness, M.B., Anderson, A.T., Martin, V.M., Maclennan, J., Passmore, E., Schwindinger, K., 2007. Textures in partially solidified crystalline nodules: a window into the pore structure of slowly cooled mafic intrusions. J. Petrol. 48, 1243–1264.

Ilyinskaya, E., Aiuppa, A., Bergsson, B., Di Napoli, R., Fridriksson, T., Óladóttir, A.A., Óskarsson, F., Grassa, F., Pfeffer, M., Lechner, K., Yeo, R., Giudice, G., 2015. Degassing regime of Hekla volcano 2012–2013. Geochim. Cosmochim. Acta 159, 80–99.

Kahl, M., Chakraborty, S., Costa, F., Pompilio, M., 2011. Dynamic plumbing system beneath volcanoes revealed by kinetic modeling, and the connection to monitoring data: an example from Mt. Etna. Earth Planet. Sci. Lett. 308, 11–22.

Kahl, M., Chakraborty, S., Costa, F., Pompilio, M., Liuzzo, M., Viccaro, M., 2013. Compositionally zoned crystals and real-time degassing data reveal changes in magma transfer dynamics during the 2006 summit eruptive episodes of Mt. Etna. Bull. Volcanol. 75, 1–14.

Kilgour, G.N., Saunders, K.E., Blundy, J.D., Cashman, K.V., Scott, B.J., Miller, C.A., 2014. Timescales of magmatic processes at Ruapehu volcano from diffusion chronometry and their comparison to monitoring data. J. Volcanol. Geotherm. Res. 288, 62–75.

Larsen, G., 2000. Holocene eruptions within the Katla volcanic system, South Iceland: characteristics and environmental impact. Jökull 49, 1–28.

Maclennan, J., 2008. Concurrent mixing and cooling of melts under Iceland. J. Petrol. 49, 1931–1953.

Martin, V.M., Davidson, J., Morgan, D., Jerram, D.A., 2010. Using the Sr isotope compositions of feldspars and glass to distinguish magma system components and dynamics. Geology 38, 539–542.

Martin, V.M., Morgan, D.J., Jerram, D.A., Caddick, M.J., Prior, D.J., Davidson, J.P., 2008. Bang! Month-scale eruption triggering at Santorini volcano. Science 321, 1178.

Métrich, N., Sigurdsson, H., Meyer, P.S., Devine, J.D., 1991. The 1783 Lakagigar eruption in Iceland – geochemistry, CO_2 and sulfur degassing. Contrib. Mineral. Petrol. 107, 435–447.

Moore, A., Coogan, L.A., Costa, F., Perfit, M.R., 2014. Primitive melt replenishment and crystal-mush disaggregation in the weeks preceding the 2005–2006 eruption 9°50′ N, EPR. Earth Planet. Sci. Lett. 403, 15–26.

Morgan, D.J., Blake, S., Rogers, N.W., De Vivo, B., Rolandi, G., Davidson, J.P., 2006. Magma chamber recharge at Vesuvius in the century prior to the eruption of AD 79. Geology 34, 845–848.

Morgan, D.J., Blake, S., Rogers, N.W., DeVivo, B., Rolandi, G., Macdonald, R., Hawkesworth, C.J., 2004. Time scales of crystal residence and magma chamber volume from modelling of diffusion profiles in phenocrysts: Vesuvius 1944. Earth Planet. Sci. Lett. 222, 933–946.

Nakamura, A., Schmalzried, H., 1983. On the nonstoichiometry and point defects of olivine. Phys. Chem. Miner. 10, 27–37.

Neave, D.A., Maclennan, J., Hartley, M.E., Edmonds, M., Thordarson, T., 2014. Crystal storage and transfer in basaltic systems: the Skuggafjöll eruption, Iceland. J. Petrol. 55, 2311–2346.

Neave, D.A., Passmore, E., Maclennan, J., Fitton, G., Thordarson, T., 2013. Crystal-melt relationships and the record of deep mixing and crystallization in the AD 1783 Laki eruption, Iceland. J. Petrol. 54, 1661–1690.

Oman, L., Robock, A., Stenchikov, G.L., Thordarson, T., Koch, D., Shindell, D.T., Gao, C., 2006. Modeling the distribution of the volcanic aerosol cloud from the 1783–1784 Laki eruption. J. Geophys. Res. 111.

Óskarsson, N., Helgason, O., Steinthórsson, S., 1994. Oxidation-state of iron in mantle-derived magmas of the Icelandic rift-zone. Hyperfine Interact. 91, 733–737.

Passmore, E., Maclennan, J., Fitton, G., Thordarson, T., 2012. Mush disaggregation in basaltic magma chambers: evidence from the AD 1783 Laki eruption. J. Petrol. 53, 2593–2623.

Ruprecht, P., Plank, T., 2013. Feeding andesitic eruptions with a high-speed connection from the mantle. Nature 500, 68–72.

Saunders, K., Blundy, J., Dohmen, R., Cashman, K., 2012. Linking petrology and seismology at an active volcano. Science 336, 1023–1027.

Saunders, K.E., Morgan, D.J., Baker, J.A., Wysoczanski, R.J., 2010. The magmatic evolution of the Whakamaru supereruption, New Zealand, constrained by a micro-analytical study of plagioclase and quartz. J. Petrol. 51, 2465–2488.

Schmidt, A., Carslaw, K.S., Mann, G.W., Wilson, M., Breider, T.J., Pickering, S.J., Thordarson, T., 2010. The impact of the 1783–1784 AD Laki eruption on global aerosol formation processes and cloud condensation nuclei. Atmos. Chem. Phys. 10, 6025–6041.

Schmidt, A., Ostro, B., Carslaw, K.S., Wilson, M., Thordarson, T., Mann, G.W., Simmons, A.J., 2011. Excess mortality in Europe following a future Laki-style Icelandic eruption. Proc. Natl. Acad. Sci. USA 108, 15710–15715.

Shishkina, T.A., Botcharnikov, R.E., Holtz, F., Almeev, R.R., Portnyagin, M.V., 2010. Solubility of H_2O- and CO_2-bearing fluids in tholeiitic basalts at pressures up to 500 MPa. Chem. Geol. 277, 115–125.

Sigmundsson, F., Hooper, A., Hreinsdóttir, S., Vogfjörd, K.S., Ófeigsson, B.G., Heimisson, E.R., Dumont, S., Parks, M., Spaans, K., Gudmundsson, G.B., Drouin, V., Árnadóttir, T., Jónsdóttir, K., Gudmundsson, M.T., Högnadóttir, T., Fridriksdóttir, H.M., Hensch, M., Einarsson, P., Magnússon, E., Samsonov, S., Brandsdóttir, B., White, R.S., Ágústsdóttir, T., Greenfield, T., Green, R.G., Hjartardóttir, Á.R., Pedersen, R., Bennett, R.A., Geirsson, H., LaFemina, P.C., Björnsson, H., Pállson, F., Sturkell, E., Bean, C.J., Möllhoff, M., Braiden, A.K., Eibl, E.P.S., 2014. Segmented lateral dyke growth in a rifting event at Bárðarbunga volcanic system, Iceland. Nature 517, 191–195.

Thomson, A., Maclennan, J., 2013. The distribution of olivine compositions in Icelandic basalts and picrites. J. Petrol. 54, 745–768.

Thordarson, T., Höskuldsson, Á., 2008. Postglacial volcanism in Iceland. Jökull 58, 197–228.

Thordarson, T., Larsen, G., 2007. Volcanism in Iceland in historical time: volcano types, eruption styles and eruptive history. J. Geodyn. 43, 118–152.

Thordarson, T., Larsen, G., Steinthorsson, S., Self, S., 2003a. The 1783–1785 AD Laki–Grímsvötn eruptions II: appraisal based on contemporary accounts. Jökull 53, 11–47.

Thordarson, T., Miller, D.J., Larsen, G., Self, S., Sigurdsson, H., 2001. New estimates of sulfur degassing and atmospheric mass-loading by the 934 AD Eldgjá eruption, Iceland. J. Volcanol. Geotherm. Res. 108, 33–54.

Thordarson, T., Self, S., 1993. The Laki (Skaftár Fires) and Grímsvötn eruptions in 1783–1785. Bull. Volcanol. 55, 233–263.

Thordarson, T., Self, S., 2003. Atmospheric and environmental effects of the 1783–1784 Laki eruption: a review and reassessment. J. Geophys. Res. 108, 4011.

Thordarson, T., Self, S., Miller, D.J., Larsen, G., Vilmundardóttir, E.G., 2003b. Sulphur release from flood lava eruptions in the Veið ivötn, Grímsvötn and Katla volcanic systems, Iceland. Geol. Soc. (Lond.) Spec. Publ. 213, 103–121.

Thordarson, T., Self, S., Óskarsson, N., Hulsebosch, T., 1996. Sulfur, chlorine, and fluorine degassing and atmospheric loading by the 1783–1784 AD Laki (Skaftár fires) eruption in Iceland. Bull. Volcanol. 58, 205–225.

Vergniolle, S., Jaupart, C., 1986. Separated two-phase flow and basaltic eruptions. J. Geophys. Res. 91, 12842–12860.

Zellmer, G.F., Blake, S., Vance, D., Hawkesworth, C., Turner, S., 1999. Plagioclase residence times at two island arc volcanoes (Kameni Islands, Santorini, and Soufriere, St. Vincent) determined by Sr diffusion systematics. Contrib. Mineral. Petrol. 136, 345–357.